Nanoscale Res Lett (2010) 5:1977–1981
DOI 10.1007/s11671-010-9735-6

NANO EXPRESS

Porous Alumina Films with Width-Controllable Alumina Stripes

Kai Huang · Shi-Ming Huang · Lin Pu · Yi Shi · Zhi-Ming Wu · Li Ji · Jun-Yong Kang

Received: 8 June 2010 / Accepted: 5 August 2010 / Published online: 21 August 2010

Abstract Porous alumina films had been fabricated by anodizing from aluminum films after an electropolishing procedure. Alumina stripes without pores can be distinguished on the surface of the porous alumina films. The width of the alumina stripes increases proportionally with the anodizing voltage. And the pores tend to be initiated close to the alumina stripes. These phenomena can be ascribed to the electric field distribution in the alumina barrier layer caused by the geometric structure of the aluminum surface.

Keywords Porous alumina films · Patterned aluminum surface · Electric field distribution · Alumina stripes

Introduction

Nanostructured materials exhibit interesting properties in a wide range of spectra including catalytic activity [1], optical properties [2] and magnetic properties [3]. Nanoporous materials with ordered structures have attracted increasing attention in recent years due to their possible utilization as templates for the organization of nanosize structures [4, 5]. One approach to the fabrication of such templates is using anodic porous alumina, which is prepared by the anodic oxidation of aluminum in various acidic electrolytes [6–9]. The degree of the ordering of the pores configuration at the surface of the porous alumina films is low because the pores develop randomly at the initial stage of the anodization. With the growth of self-organized pores, a densely packed hexagonal pore structure is established gradually. An explosion of porous alumina research was ignited once the capability of producing a nanohole array with excellent regularity was established by Masuda et al. [6]. Highly ordered anodic alumina films have been mostly achieved by the two-step anodizing the aluminum after electropolishing in perchloric acid–alcohol solution. The highly ordered anodic alumina films play important roles in many fields such as photonic crystals and magnetic interaction [10–14]. Recently, another anodic porous photoelectric material, the porous TiO_2, acquired highly ordered structure through the two-step anodizing procedure after electropolishing [15].

In order to improve the degree of order, shorten the fabrication time and fabricate non-hexagonal structure porous alumina films, surface prepatterning by different physical techniques has been found by Masuda et al. [16–18]. This plays its role at the nucleation stage of pore formation as the pores are initiated directly at the troughs of prepatterned surface. It suggests that the nanoscale surface morphology or nanotexture of the aluminum surface before anodizing is important for further pore formation stage. In most works, pores are initiated directly at the troughs of the pretextured surface. But in some cases, the pores are also initiated at unexpected sites between prepatterned troughs [19, 20].

Here, we investigate the surface morphology of porous alumina films after the aluminum anodizing procedure on the electrochemically polished aluminum surface. The morphology of a cellular aluminum surface fabricated by the electropolishing process can be transferred to the anodic alumina surface. There exist alumina stripes without

K. Huang (✉) · Z.-M. Wu · L. Ji · J.-Y. Kang
Semiconductor Photonics Research Center, Department of Physics, Xiamen University, 361005 Xiamen, China
e-mail: k_huang@xmu.edu.cn

S.-M. Huang · L. Pu · Y. Shi
Key Laboratory of Photonic Electronic Materials, Nanjing University, 210093 Nanjing, China

pores on the surface of porous alumina films. And the stripes comprise cells [21]. The width of stripes increases proportionally with the anodizing voltage. The pores present on the remaining part of surface tend to initiate close to the stripes rather than the middle of the center of the cell. These can be ascribed to the electric field distribution in the alumina barrier layer caused by the geometric structure of the aluminum surface.

Experimental Section

Porous alumina films were made by anodizing aluminum foils (99.999%, 0.5-mm thick). After annealing under N_2 ambient at 450°C for 4 h, aluminum foil was ultrasonically degreased in acetone for 5 min and then it was electrochemically polished in a mixture solution of $HClO_4$ and C_2H_5OH with a volume ratio of 20:80 at a current density of 100mAcm-2 for several times (first time 2 min, second time 5 min and third time 15 min). The polished aluminum foil was placed on the anode (Cu plate) and anodized in certain electrolyte at 5°C for 10 min. A Pt wire served as the cathode. The anodizing voltages are 30, 40, 50 and 60 V in 0.3 M oxalic acid (sample A, B, C and D, respectively) and 5, 15 V in 15wt% sulfuric acid. The morphology of the polished aluminum surface was measured using AFM (NanoScope IIIa). The sample morphology was observed using a SEM (LEO 1530VP).

Results and Discussion

Figure 1a–d shows the typical surface SEM image of the top surface of the sample A–D, respectively. In Fig. 1b, a mass of pores of 30–40 nm are observed at the top surface, which is in agreement with other authors who have used the same fabrication condition [22]. However, disparate with prevalent reports, there are many cells that consist of protuberant stripes observed on the surface. The origin of the stripes has been discussed in the prior report [21]. The average width of the stripes is about 56 nm. The average diameter of the cells is about 200 nm. While observing the exact location of the pores, we can find that the pores are initiated non-uniform. Pores tend to be initiated at the region close to the protuberant stripes. Most pores mainly distribute in the region with the distance about 30–40 nm to the midline of stripes (i.e., pore a in the denoted cell) and there is almost one pore locating at each angle of each cell

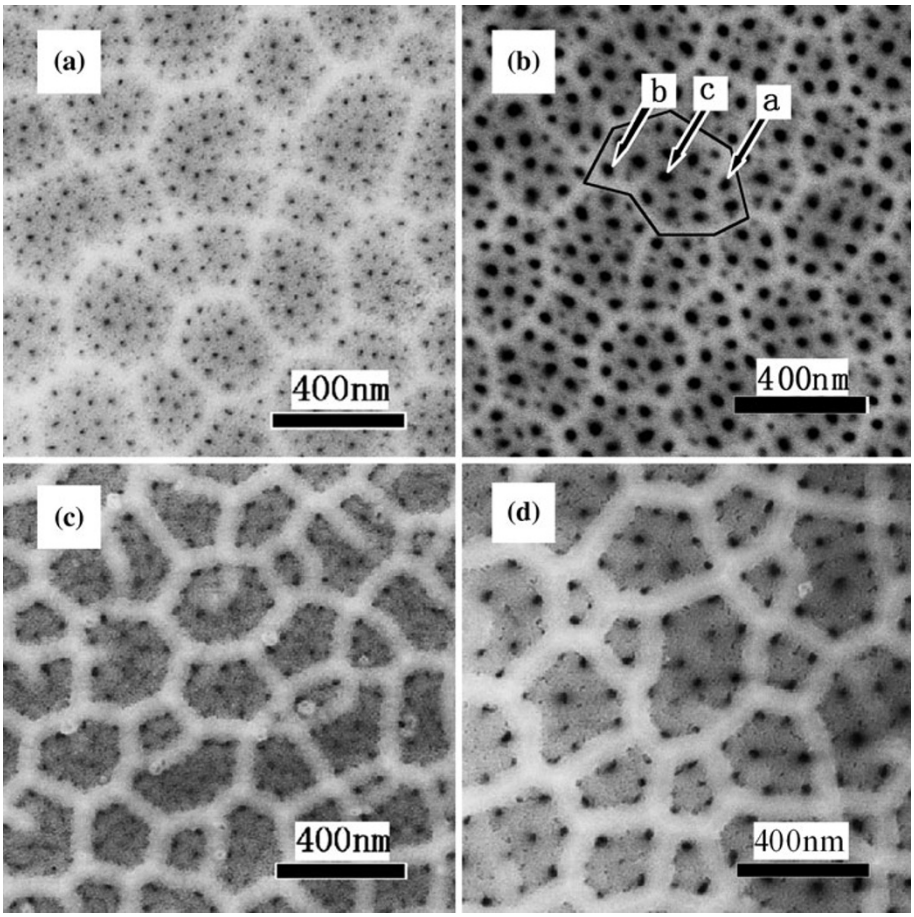

Fig. 1 The surface morphology of the porous alumina films under different anodizing voltages **a** 30 V, **b** 40 V, **c** 50 V, **d** 60 V in oxalic acid, respectively

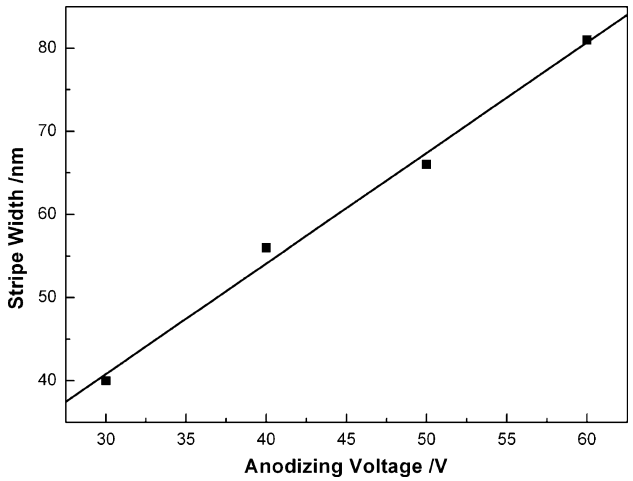

Fig. 2 Linear dependence between the average stripe width and the anodizing voltage

(i.e., pore b). Only few pores locate at the middle of the polygons (i.e., pore c). Statistically, there is 0% pore locating at the stripes region, which holds 30% of the total area of the surface, about 80% pores locating at the region close to the stripes, which holds about 45% of the total area of the surface. However, there are only 20% pores locating at the middle of the cells, which holds about 25% of the total area of the surface. These data indicate that the pores initiation shows significant non-uniformity.

The surface morphology of sample ACD seems to be similar to sample B. The difference of these samples is the pore density and the stripe width. The average stripe widths of sample A, B, C and D are 40, 56, 66 and 81 nm, respectively, and Fig. 2 is the linear dependence between the average stripe width and the anodizing voltage.

The Fig. 2 indicates that the stripe width increases proportionally with the anodizing voltage. It can be assumed that this phenomenon would result from the non-uniformity of the electric field caused by the non-planar anodizing procedure of aluminum. Figure 3 shows the SEM and AFM image of aluminum surface after being electropolished in perchloric acid–alcohol solution. Cellular pattern can be observed on the aluminum surface. The average diameter of the cells is about 200 nm. The boundary of cells is formed by protuberant aluminum stripes. And it can be measured from the AFM image that the height of the stripes is about 20 nm. This cellular pattern on the aluminum surface is caused by the

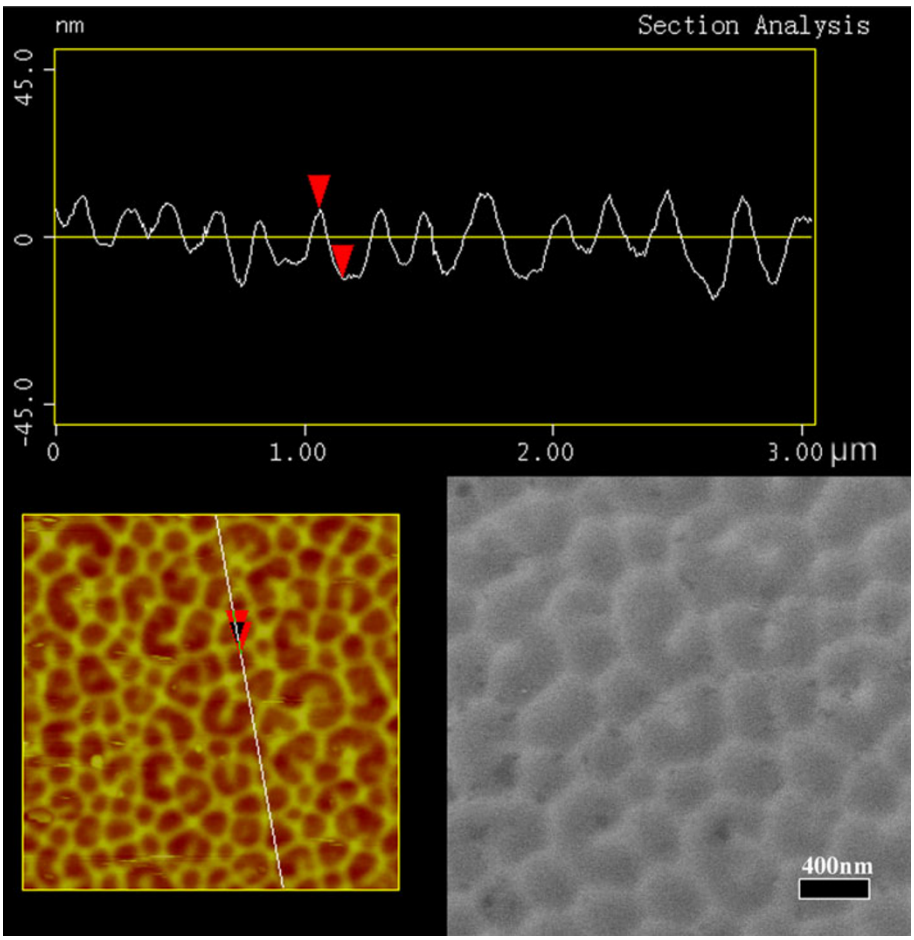

Fig. 3 AFM (*top* and *lower left*) and SEM (*lower right*) image of aluminum surface after being electropolished in perchloric acid–alcohol solution

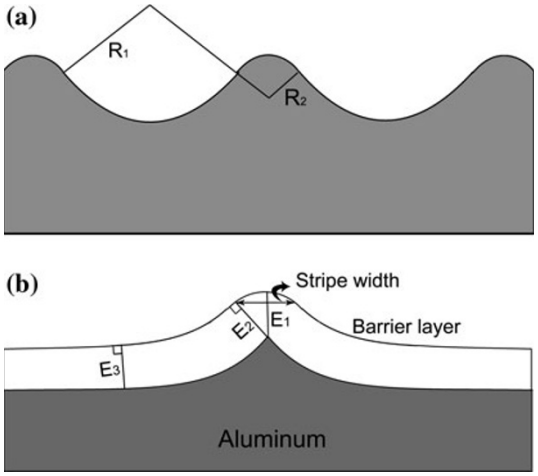

Fig. 4 **a** Schematic diagram of the patterned surface of aluminum after electropolishing, **b** schematic diagram of the patterned surface and the barrier layer structures of the barrier layer formed at the initial stage of anodizing

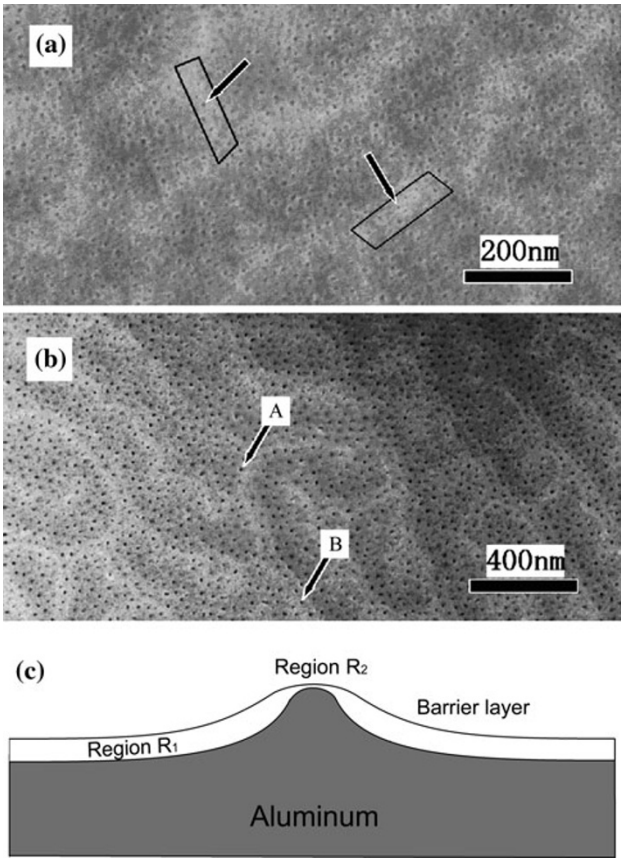

Fig. 5 **a** The surface morphology of the porous alumina films under the anodizing voltage of 5 V, **b** the surface morphology of the porous alumina films under the anodizing voltage of 15 V, **c** schematic diagram of the barrier layer structures formed at the initial stage of anodizing at a relatively low voltage

electropolishing procedure [23]. It can be seen easily that these features of the cells on the aluminum surface are quite similar to the cells on the alumina surface after further anodizing procedure. Thus, it can be deduced that the alumina stripes after anodizing procedure originate from the former aluminum stripes.

The initial stage of anodizing on patterned aluminum surface is schematically shown in Fig. 4. Figure 4a shows the patterned aluminum surface after electropolishing procedure. This can be approximately regarded as a structure consisting of a negative curvature region on which $R = R_1$ (denoted as region R_1) and a positive curvature region on which $R = R_2$ (denoted as region R_2). It can be deduced from the AFM image that the R_1 is much bigger than R_2. During the first few seconds of the constant voltage anodizing, the current decreases rapidly. A thin barrier layer–type alumina forms at this stage [21]. The thickness of the barrier layer is about $1.4 \times V$ nm, where V is the applying anodizing voltage. The sketch of the barrier layer has been shown as Fig. 4b. According to the Gaussian's law, the electric field intensity of the point with a distance r from point A can be approximatively regarded as $E_1 \sim \frac{\sigma r_a}{\varepsilon r}$, where σ is the electric charge density of point A, ε is the dielectric constant of alumina and r_a is the curvature radius on point A. The geometry indicates that on the electrolyte/alumina interface, $r_a \ll r$, so it can be deduced that $E_1 \ll \frac{\sigma}{\varepsilon}$. Therefore, the pores cannot be initialized on the region R_2. And then, region R_2 forms the alumina stripes. Where at the tie point of region R_1 and region R_2, the intensity of the electric field can be approximatively regarded as $E_2 \sim \frac{\sigma}{\varepsilon}$. Under the static electric field assumption, the electric charge density on the region R_2 is much bigger than on the region R_1. Therefore, the electric field intensity is much bigger on region R_2 ($E_2 \gg E_3$). Thus, we can obtain the reason why the pore density of the region close to the stripes is much higher than the region in the middle of the cells. Therefore, pores tend to be initialized at the tie point of the region R_1 and region R_2, i.e., the brink of the stripes. It can also explain the pore-in-pore structures referred by Zhu et al. [24]. We can see from the geometric structure that the width of the alumina stripes is proportional to the thickness of the barrier layers or the anodizing voltage as shown in Fig. 1.

While the applying anodizing voltage is rather low, the surface morphology of the porous alumina films become totally different. Figure 5a shows the surface SEM image of the porous alumina under a very low anodizing voltage of 5 V. It can be distinguished that there are protuberant stripes showed in the surface (i.e., quadrilateral marked in Fig. 5a). But pores do not avoid the stripe region as discussed above. By contraries, there are a lot of pores located at the midline of the stripes (i.e., pore indicated in Fig. 5a). Figure 5b shows the differentiation of the

surface morphology of the porous alumina under the anodizing voltage of 15 V. Some pores form at the border of the stripes (pore A) and there are still some pores locating at the middle of the stripes (pore B). When the anodizing voltage is relatively low (lower than R_2/1.1 nm/V), it can be deduced that the barrier layer forms the structure as Fig. 5c. Under the static electric field assumption, the electric charge density on the region R_2 is much bigger than on the region R_1. Therefore, the electric field intensity is bigger on region R_2. The thickness of the barrier can be estimated by the equation $\int E \cdot \mathrm{d}l = V$. Thus, we can draw the conclusion that the barrier layer on region R_2 is much thinner than that on region R_1. Along with the anodizing proceeding, microcracks caused by the stress and the heat on region R_2 can be much easier to impenetrate the hole barrier layer and then form the pores. That is, in the case of a rather small anodizing voltage, the pores tend to initiate on the positive curvature region i.e., on the stripes.

Conclusions

In conclusion, porous alumina films were fabricated by anodizing from films of aluminum after an electropolishing procedure. Alumina stripes can be distinguished on the surface of the porous alumina. The width of the alumina stripes increases proportionally to the anodizing voltage. And the pores tend to be initiated close to the alumina stripes. These phenomena were ascribed to the non-uniformity of the electric field caused by the non-planar anodizing procedure of aluminum. We believe that this mechanism is not a special case but just surface geometric structure related. And further, it can result in a new method for prognosticating the surface structure of the porous alumina films.

Acknowledgments The authors are grateful to the Natural Science Foundation of Fujian Province of no. 2008J0029.

References

1. H. Habazaki, M. Yamasaki, A. Kawashima, K. Hashinoto, Appl. Organomet. Chem. **14**, 803 (2000)
2. A.G. Cullis, L.T. Canham, P.D.J. Calcott, J. Appl. Phys. **82**, 909 (1997)
3. G. Herzer, IEEE Trans. Magn. **25**, 3327 (1989)
4. R.J. Tonucci, B.L. Justus, A.J. Campillo, C.E. Ford, Science **258**, 783 (1992)
5. T.M. Whitney, J.S. Jiang, P.C. Searson, C.L. Chien, Science **261**, 1316 (1993)
6. H. Masuda, K. Fukuda, Science **268**, 1466 (1995)
7. H. Masuda, F. Hasegwa, S. Ono, J. Electrochem. Soc. **144**, L127 (1997)
8. H. Masuda, K. Yada, A. Osaka, Jpn. J. Appl. Phys. **37**, L1340 (1998)
9. A.P. Li, F. Muller, A. Birner, K. Nielsch, U. Gösele, J. Appl. Phys. **84**, 6023 (1998)
10. V. Kuzmiak, A.A. Maradudin, F. Pincemin, Phys. Rev. B **50**, 16835 (1994)
11. H. Masuda, M. Ohya, K. Nishio, H. Asoh, M. Nakao, M. Nohtomi, T. Tamamura, Jpn. J. Appl. Phys. **39**, L1039 (2000)
12. J. Choi, Y. Luo, R.B. Wehrspohn, R. Hillebrand, J. Schilling, U. GöSele, J. Appl. Phys. **94**, 4757 (2003)
13. V. Raposo, J.M. Garcia, J.M. Gonzalez, M. Vázquez, J. Magn. Magn. Mater. **222**, 227 (2000)
14. H.R. Khan, K. Petrikowski, J. Magn. Magn. Mater. **215–216**, 526 (2000)
15. Y. Shin, S. Lee, Nano Lett. **8**, 3171 (2008)
16. H. Masuda, H. Yamada, M. Satoh, H. Asoh, M. Nakao, T. Tamamura, Appl. Phys. Lett. **71**, 2770 (1997)
17. H. Masuda, H. Asoh, M. Watanabe, K. Nishio, M. Nakao, T. Tamamura, Adv. Mater. **13**, 189 (2001)
18. Z.J. Sun, H.K. Kim, Appl. Phys. Lett. **81**, 3458 (2002)
19. H. Masuda, M. Yotsuya, M. Asano, K. Nishio, M. Nakao, A. Yohoo, T. Tamamura, Appl. Phys. Lett. **78**, 827 (2001)
20. J. Choi, K. Nielsch, M. Reiche, R.B. Wehrspohn, U. Gösele, J. Vac. Sci. Technol. B **21**(2), 763 (2003)
21. G.E. Thompson, Thin Solid Films **297**, 192 (1997)
22. K. Nielsch, J. Choi, K. Schwin, R.B. Wehrspohn, U. Gösele, Nano Lett. **2**, 677 (2002)
23. R.E. Ricker, A.E. Miller, D.F. Yue, G. Banerjee, S. Bandyopadhyay, J. Electron. Mater. **25**, 1585 (1996)
24. Y.Y. Zhu, G.Q. Ding, J.N. Ding, N.Y. Yuan, Nanoscale Res. Lett. **5**, 725 (2010)